Implementation of ternary Shor's algorithm based on vibrational states of an ion in anharmonic potential*

Liu Wei(刘 威)[a)b)†], Chen Shu-Ming(陈书明)[a)b)], Zhang Jian(张 见)[a)b)], Wu Chun-Wang(吴春旺)[c)], Wu Wei(吴 伟)[c)], and Chen Ping-Xing(陈平形)[c)]

[a)] College of Computer, National University of Defense Technology, Changsha 410073, China
[b)] Science and Technology on Parallel and Distributed Processing Laboratory (PDL), National University of Defense Technology, Changsha 410073, China
[c)] College of Science, National University of Defense Technology, Changsha 410073, China

(Received 3 June 2014; revised manuscript received 28 October 2014; published online 19 January 2015)

It is widely believed that Shor's factoring algorithm provides a driving force to boost the quantum computing research. However, a serious obstacle to its binary implementation is the large number of quantum gates. Non-binary quantum computing is an efficient way to reduce the required number of elemental gates. Here, we propose optimization schemes for Shor's algorithm implementation and take a ternary version for factorizing 21 as an example. The optimized factorization is achieved by a two-qutrit quantum circuit, which consists of only two single qutrit gates and one ternary controlled-NOT gate. This two-qutrit quantum circuit is then encoded into the nine lower vibrational states of an ion trapped in a weakly anharmonic potential. Optimal control theory (OCT) is employed to derive the manipulation electric field for transferring the encoded states. The ternary Shor's algorithm can be implemented in one single step. Numerical simulation results show that the accuracy of the state transformations is about 0.9919.

Keywords: ternary Shor's algorithm, anharmonic ion trapping, optimal control theory, vibrational state

PACS: 37.10.Ty, 03.67.Ac, 03.67.Lx **DOI:** 10.1088/1674-1056/24/3/033701

1. Introduction

One of the main focal aspects of modern science is the realization of a full-scale quantum computer.[1–7] It is widely believed that Shor's factoring algorithm provides a driving force to boost quantum computing research. In theory, factorizing N by a full-scale Shor's algorithm could be achieved by about $72\lceil\log_2 N\rceil^3$ binary quantum gates.[8] In practice, the large number of quantum gates places a serious obstacle to the algorithm's implementation. According to the present technologies, small-scale quantum computing devices built on a variety of physical systems exist in the laboratory and have demonstrated the fundamental characteristics for building systems. On the nuclear magnetic resonance system, 15 is factorized.[9] The same work is also demonstrated on a photonic system[10] and on a photonic chip.[11] These are binary demonstrations. Binary quantum computation is built upon the quantum bit (or qubit for short), which is a two-level quantum system that can be represented mathematically by a vector in a two-dimensional Hilbert space.[12] Realizing qubits usually enforces a two-level structure on systems by convention and not by physical reality, which is naturally far more complex and has many readily accessible degrees of freedom.

Nowadays, higher-dimensional quantum systems with more degrees of freedom have been studied, which can exponentially extend the Hilbert space on the same system.[13] For example, the Toffoli gate is simplified by involving a third level of the qubits.[14] Higher-dimensional systems enable the evolution from binary (qubit) to non-binary (qudit) quantum computing.[15] The main advantage of non-binary computing is the exponential increases of speed and capacity when increasing the encoding elements,[16] thus significantly reducing the number of elemental gates required to build key quantum circuits.[14,17,18] The scheme introduced in Ref. [19] is an appropriate model to study non-binary quantum computing because it allows control of the vibrational states of an ion adiabatically using electric fields. A progression of several vibrational states can be employed to execute simple quantum algorithms using a single trapped ion. The state-to-state transitions between vibrational states of the ion are slightly anharmonic, thus occur at slightly different frequencies and can be controlled selectively. In such a scenario, the frequency content of shaped electric fields should be in the MHz range. In recent years, several anharmonic ion traps have been shown to be suitable for practical implementation.[20–24]

In this paper, we propose optimization schemes for Shor's algorithm implementation and take a ternary version for factorizing 21 as an instantiation. It turns out that the specific factorization is achieved by a two-qutrit quantum circuit, which consists of only two single qutrit gates and one ternary controlled-NOT (TCNOT) gate. This is a representative advantage compared to the previous studies.[10,11] By randomly choosing 4 as the base in our implementation, the

*Project supported by the National Natural Science Foundation of China (Grant No. 61205108) and the High Performance Computing (HPC) Foundation of National University of Defense Technology, China.

†Corresponding author. E-mail: wliu@nudt.edu.cn

© 2015 Chinese Physical Society and IOP Publishing Ltd

period of the modular exponential function is 3, i.e., the order is 3. Traditionally, the orders of the previous studies[10,11] are even integers. Our implementation technique is independent of the physical encoding of quantum information and the way in which the elemental gates are themselves constructed. Therefore, we encode the two-qutrit quantum circuit into the lower nine vibrational states of the trapped ion.[19] Optimal control theory (OCT) is employed to derive the manipulation field for transferring the encoded states. The manipulation can be achieved in two ways: separately implement the elementary ternary gates step-by-step or implement the whole algorithm in one step.[25] Numerical simulation results show that the accuracy of the state transformations is about 0.9919 for the one step implementation.

The remainder of this paper is organized as follows. In Section 2 we discuss optimization process of the ternary Shor's algorithm. In Section 3 we briefly review the theoretical model and major properties of one ion trapped in anharmonic potential. Section 4 outlines the control problem and the OCT solution to it. The results of the OCT calculations are presented and analyzed in Section 5. Finally, Section 6 provides our conclusion.

2. Ternary Shor's algorithm

Shor's algorithm switches the factoring problem to the problem of finding the period of a function. Quantum parallelism is utilized to obtain a superposition of all of the values of the function in one step. The quantum Fourier transform of the function is then computed, thus all of the amplitude of the function is put into multiples of the reciprocal of the period. The period, or the order which in turn is used to factor the integer N, is obtained through high probability measurement of the state. The order-finding part of the algorithm is the kernel, which has been experimentally demonstrated.[9–11] However, the orders employed in the previous studies were a power of 2.[9–11] In this section, we generalize the d-dimensional order-finding procedure and optimize the number of qudits, we then factorize 21 by a ternary version to show that an odd order is also feasible.

Theorem 1 The d-dimensional order-finding procedure uses two registers: an argument register and a function register, which consist of $\lceil 2\log_d N\rceil$ qudits and $\lceil \log_d N\rceil$ qudits, respectively.

Proof The main component of the quantum order-finding is the modular exponentiation computing the function of $a^x \pmod N$, where a is a random number chosen from the set $\{1<a<N\} \bigcap \gcd(a,N) = 1$, and x is the argument of the function taking values between 0 and at least N^2. So, in order to hold a modulo N integer in the function register, $\lceil \log_d N\rceil$ qudits is needed. In addition, the argument register needs to hold at least N^2 arguments. Through logarithm conversion with base d, we can get that $\lceil 2\log_d N\rceil$ qudits are necessary.

Example Suppose that ternary Shor's algorithm were implemented to factor 21. $\lceil \log_3 21\rceil = 3$ qutrits are in the function register. The argument register consists of 6 qutrits ($3^5 = 243 < 21^2 = 441 < 3^6 = 729$), as shown in Fig. 1(a). However, 9 qubits and 5 qubits are needed in the two quantum registers for the traditional binary order-finding algorithm.[26] The first step of the procedure is preparation of the argument register in an equally weighted coherent superposition state. This is usually achieved by Hadamard gates. The d-dimensional Hadamard gate is defined as $H^{(d)}|l\rangle = \sum_{j=0}^{d-1} \mathrm{e}^{\mathrm{i}2\pi jl/d}|j\rangle/\sqrt{d}$. The matrix form of the ternary Hadamard gate is

$$H^{(3)} = \frac{1}{\sqrt{3}}\begin{pmatrix} 1 & 1 & 1 \\ 1 & \mathrm{e}^{\mathrm{i}2\pi/3} & \mathrm{e}^{-\mathrm{i}2\pi/3} \\ 1 & \mathrm{e}^{-\mathrm{i}2\pi/3} & \mathrm{e}^{\mathrm{i}2\pi/3} \end{pmatrix}. \tag{1}$$

In addition, the following Theorems 2 and 3 show that the number of qudits can be ulteriorly reduced under certain circumstance.

Theorem 2 With pre-determined N and a, if $a^{d^m} \pmod N = 1$, the necessary $n = \lceil 2\log_d N\rceil$ qudits in argument register can be reduced to m ($0 < m < n$). Otherwise, such reduction fails.

Proof $a^x = a^{d^{n-1}x_{n-1}} \cdots a^{d^1 x_1} a^{d^0 x_0}$, thus modular exponentiation consists of serial multiplication by $a^{d^k} \pmod N$ for all k, where $0 \le k < n$. If $a^{d^m} \pmod N = 1$, thus all $a^{d^k} \pmod N = 1$ for $k \ge m$. In this case, $a^x \pmod N$ simplifies to multiplications controlled by just m qudits.

Example Suppose that $a = 4$ is randomly chosen. As shown in Fig. 1(a), $4^x \pmod{21}$ can be easily accomplished using 6 consecutive controlled multiplications $4^{3^i x_i} \pmod{21}$, where i = 0, 1,..., 5. It is clear that $4^3 \pmod{21} = 1$, thus, the high-orders, $4^{3x_1} \pmod{21}$,..., $4^{3^5 x_5} \pmod{21}$, are redundant in Fig. 1(a). Such simplification ulteriorly reduces the number of qutrits used in the argument register from 6 to 1. We can then apply the inverse quantum Fourier transform (InvQFT$^{(3)}$) to the argument register, followed by a measurement of the population of the qutrit states. One qutrit inverse Fourier transform is also achieved by a ternary Hadamard gate, which is shown in Eq. (1).

Theorem 3 With pre-determined N and a, if the period of modular exponentiation r is odd, then $\sqrt{a}$ should be an integer. In addition, if $r = d$, then the necessary $\lceil \log_d N\rceil$ qudits in function register can be reduced to 1. Otherwise, such reduction fails.

Proof Generally, after r is obtained, it needs to compute $\gcd(a^{r/2}-1, N)$ and $\gcd(a^{r/2}+1, N)$, and test to see if this is a non-trivial factor. Hence, $a^{r/2}$ needs to be an integer, i.e., $\sqrt{a}$ is an integer. In addition, $r = d$ means that $a^{0,1,\ldots,d-1}$ are different to each other. Then $\log_a(a^{0,1,\cdots,d-1}) = 0, 1, \ldots, d-1$, which happens to be the d basis states of a qudit.

Example For a control qutrit, x_0 = 0, 1, 2. i.e., the controlled modular multiplication $4^{x_0} \pmod{21}$ = 1, 4, 16, and $4^3 \pmod{21} = 1$, i.e., the period $r = d = 3$. Hence, $\log_4(4^{x_0})$ = 0, 1, 2 is obtained. The number of qutrits used in the function

register is reduced from 3 to 1. This conclusion switches the control modular multiplication to the TCNOT shown as[13]

$$\text{TCNOT} = \begin{pmatrix} 1&0&0&0&0&0&0&0&0 \\ 0&1&0&0&0&0&0&0&0 \\ 0&0&1&0&0&0&0&0&0 \\ 0&0&0&0&0&1&0&0&0 \\ 0&0&0&1&0&0&0&0&0 \\ 0&0&0&0&1&0&0&0&0 \\ 0&0&0&0&0&0&0&1&0 \\ 0&0&0&0&0&0&0&0&1 \\ 0&0&0&0&0&0&1&0&0 \end{pmatrix}. \quad (2)$$

Above all, figure 1(b) shows the implementation of Theorems 2 and 3.

Note that the scalability of the Theorems 2 and 3 is based on a certain circumstance, i.e., N and a are pre-determined. With the presence of such a precondition, we can classically compute other parameters, such as r and d, to design experiments.

The two-qutrit quantum circuit in Fig. 1(b) can be achieved in two ways: separately implement the three gates step-by-step or implement the whole algorithm in one step. In the following Section 3, the two-qutrit system is encoded into the nine lower vibrational states of an ion trapped in anharmonic potential. Similarly to the TCNOT, $H^{(3)}$ and Inv$H^{(3)}$ should be expanded by adding the needed identity matrix to create the 9×9 matrices: $H^{(3)} \otimes I^{(3)}$ and Inv$H^{(3)} \otimes I^{(3)}$. The three unitary operation can be applied to the two-qutrit system step-by-step, or the whole order-finding algorithm can be represented by a single 9×9 unitary matrix: $U = (\text{Inv}H^{(3)} \otimes I^{(3)})\cdot\text{TCNOT}\cdot(H^{(3)} \otimes I^{(3)})$. The final result is

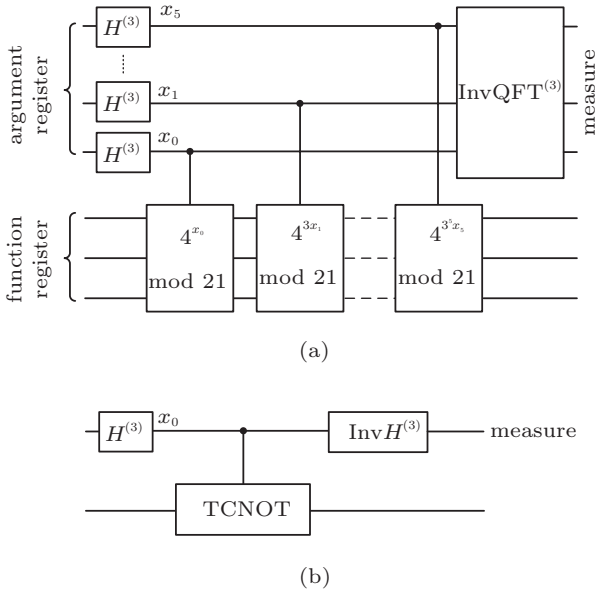


Fig. 1. Quantum circuit for the order-finding algorithm. (a) Ternary order-finding algorithm for factoring 21 with order 3, and the positive integer, which is a co-prime to 21, is randomly chosen to be 4. (b) Simplified circuit.

$$U = \frac{1}{3}\left(\begin{array}{ccc|ccc|ccc} 1 & 1 & 1 & 1 & e^{-i2\pi/3} & e^{i2\pi/3} & 1 & e^{i2\pi/3} & e^{-i2\pi/3} \\ 1 & 1 & 1 & e^{i2\pi/3} & 1 & e^{-i2\pi/3} & e^{-i2\pi/3} & 1 & e^{i2\pi/3} \\ 1 & 1 & 1 & e^{-i2\pi/3} & e^{i2\pi/3} & 1 & e^{i2\pi/3} & e^{-i2\pi/3} & 1 \\ \hline 1 & e^{i2\pi/3} & e^{-i2\pi/3} & 1 & 1 & 1 & 1 & e^{-i2\pi/3} & e^{i2\pi/3} \\ e^{-i2\pi/3} & 1 & e^{i2\pi/3} & 1 & 1 & 1 & e^{i2\pi/3} & 1 & e^{-i2\pi/3} \\ e^{i2\pi/3} & e^{-i2\pi/3} & 1 & 1 & 1 & 1 & e^{-i2\pi/3} & e^{i2\pi/3} & 1 \\ \hline 1 & e^{-i2\pi/3} & e^{i2\pi/3} & 1 & e^{i2\pi/3} & e^{-i2\pi/3} & 1 & 1 & 1 \\ e^{i2\pi/3} & 1 & e^{-i2\pi/3} & e^{-i2\pi/3} & 1 & e^{i2\pi/3} & 1 & 1 & 1 \\ e^{-i2\pi/3} & e^{i2\pi/3} & 1 & e^{i2\pi/3} & e^{-i2\pi/3} & 1 & 1 & 1 & 1 \end{array}\right). \quad (3)$$

3. The model system

Considering one single ion trapped in a Paul trap. The radio-frequency electrodes have an oscillating voltage applied to them, the others are applied with static voltages. The trapping potentials are arranged such that the ion is confined more strongly in the radial directions than in the axial direction.[20] Such a system is essentially one-dimensional. The position of the ion is given by axial coordinate z, measured here in the atomic units of length (which is the Bohr radius, r_0). In the harmonic potential trap it is well-known that the frequencies between different energy levels are all the same. After a slight anharmonic potential is added, selectively addressing and controlling the transitions between two specific energy levels of the ion become feasible by applying a spatially homogeneous field with time-dependent amplitude $\varepsilon(t)$.[19] Traditionally, the analytical anharmonic potential has the form of $\phi = kz^2/2 + k'z^4/4!$,[20] where the coefficients k and k' represent two force constants. The parameters used in this paper are determined by mimicking the previous studies,[19,27] where a $^{111}Cd^+$ ion is trapped with the axial (harmonic) frequency of $\omega/2\pi = 2.77$ MHz. According to $k = m\omega^2$, $k/2\pi = 1.483 \times 10^{-3}$ MHz/r_0^2. The anharmonic

term $k'/2\pi = 1.067 \times 10^{-7}$ MHz/r_0^4 is chosen.

Based on the above parameters, energy eigenvalues of the lower ten vibrational states (E) and transition dipole moments (the bold numbers) are calculated and summarized in Table 1, which are then used in the following OCT calculation. Details of the calculation can be found in Ref. [27]. Although the added anharmonicity is relatively small, the effect of anharmonicity can be easily spotted from the transition frequencies. The transition frequency for excitation of one quantum of vibration increases as the vibrational state number increases. For example, for a single excitation of the lowest vibrational state the frequency is $\omega_{0,1}/2\pi = 2.8151$ MHz, while for the 10th state it is $\omega_{9,10}/2\pi = 3.1224$ MHz, which is about 10.9% higher. A transition dipole moment is used to measure the transition degree between states v and v', which can be calculated as $M_{v,v'} = \langle \Psi_v(z)|qz|\Psi_{v'}(z)\rangle$, where $\Psi_v(z)$ is the wave function of state v. Note that the dipole moments are clearly dominated by $\triangle v = \pm 1$ transitions, as shown in Table 1, which is consistent with the slight anharmonicity of the system. For example, the matrix element $M_{0,1} = 30.3181 er_0$ is two orders of magnitude larger than the element $M_{0,3} = 9.47 \times 10^{-2} er_0$, which in turn is two orders of magnitude larger than $M_{0,5} = 4.98 \times 10^{-4} er_0$. In the whole paper, the two-qutrit system is encoded into the nine lower vibrational states, as shown in the first row of Table 1. The 10th abundant state ($|\text{unused}\rangle$) is also involved to avoid reflection of the upper states.

4. OCT pulse optimization

In order to obtain the electric field $\varepsilon(t)$ for transferring from a given initial state $\Psi_v(z)$ to a chosen target vibrational state $\Psi_{v'}(z)$, or to a superposition of states $\sum c_{v'}\Psi_{v'}(z)$, the OCT of Rabitz[28,29] is employed to maximize the objective functional

$$J = \frac{1}{K}\sum_{k=1}^{K} |\langle \psi_i^k(T)|\Psi_{v'}^k\rangle|^2 - \alpha \int_0^T \frac{\varepsilon^2(t)}{s(t)}\,\mathrm{d}t - 2\sum_{k=1}^{K} \mathrm{Re}\left\{ \langle \psi_i^k(T)|\Psi_{v'}^k\rangle \int_0^T \langle \psi_f^k(t)|\mathrm{i}H_{\mathrm{ion}} + \frac{\partial}{\partial t}|\psi_i^k(t)\rangle\,\mathrm{d}t \right\}, \quad (4)$$

where $\psi_i(t)$ and $\psi_f(t)$ are the time-dependent wave functions driven by $\varepsilon(t)$ forward and backward, respectively. The first term in Eq. (4) represents an overlap of the final wave function with the target state and it is maximized; the second term is required to minimize energy of the field and constrain its smooth switching on and off; and, the last term ensures that evolution of the wave functions satisfies the time-dependent Schrödinger equations $\mathrm{i}\partial\psi^k(t)/\partial t = H_{\mathrm{ion}}\psi^k(t)$, where

$$H_{\mathrm{ion}} = -\frac{\hbar^2}{2m}\frac{\partial^2}{\partial z^2} + q\phi - \varepsilon(t)qz.$$

The electric

$$\varepsilon(t) = -\frac{s(t)}{\alpha}\sum_{k=1}^{K} \mathrm{Im}\langle \psi_i^k(t)|\psi_f^k(t)\rangle\langle \psi_f^k(t)|qz|\psi_i^k(t)\rangle$$

permits one to determine the optimal $\varepsilon(t)$ iteratively.

We start with a guess electric $(A\sin(|E_{v'} - E_v|t)\sin^2(\pi t/T))$ and improve its shape iteratively by propagating the time-dependent Schrödinger equations forward and backward in time until the convergence is achieved. At the end of each backward propagation, new values of the electric field are updated and then used for the forward propagation, as well as in turn. The initial and target states of forward and backward propagation are mutual. Note that propagation performance depends somewhat on the penalty factor α.[30] In the following numerical calculations in Section 5, the wave packet is expanded in the basis set of ten vibrational eigenstates. The amplitude of the guess pulse A is set to 10 mV/cm, penalty factor α is chosen to be between 1×10^{12} and 4×10^{12}. The number of forward–backward iterations for convergence is set to 10000.

Usually, multiple state-to-state transformations are optimized simultaneously. For example, for a TCNOT gate (in

Table 1. Relevant vibrational energy levels and transition dipole moments for ten lower vibrational states in the model system of an ion trapped in weakly anharmonic potential. The qutrit state assignments are shown in the first row. The energies of eigenvalues $E/2\pi$ are in units of MHz. The values of the dipole moment are in units of er_0.

Qutrits state		$\|00\rangle$	$\|01\rangle$	$\|02\rangle$	$\|10\rangle$	$\|11\rangle$	$\|12\rangle$	$\|20\rangle$	$\|21\rangle$	$\|22\rangle$	unused
v: vibrational		0	1	2	3	4	5	6	7	8	9
state	$E/2\pi$	1.3964	4.2115	7.0702	9.9707	12.9115	15.8910	18.9079	21.9611	25.0494	28.1718
0	1.3964	0.0000	**30.3181**	0.0000	**0.0947**	0.0000	**0.0010**	0.0000	0.0000	0.0000	0.0000
1	4.2115	**30.3181**	0.0000	**42.5473**	0.0000	**0.1806**	0.0000	**0.0010**	0.0000	0.0000	0.0000
2	7.0702	0.0000	**42.5473**	0.0000	**51.7310**	0.0000	**0.2729**	0.0000	**0.0020**	0.0000	0.0000
3	9.9707	**0.0947**	0.0000	**51.7310**	0.0000	**59.3217**	0.0000	**0.3697**	0.0000	**0.0030**	0.0000
4	12.9115	0.0000	**0.1806**	0.0000	**59.3217**	0.0000	**65.8878**	0.0000	**0.4693**	0.0000	**0.0040**
5	15.8910	**0.0010**	0.0000	**0.2729**	0.0000	**65.8878**	0.0000	**71.7235**	0.0000	**0.5707**	0.0000
6	18.9079	0.0000	**0.0010**	0.0000	**0.3697**	0.0000	**71.7235**	0.0000	**77.0050**	0.0000	**0.6730**
7	21.9611	0.0000	0.0000	**0.0020**	0.0000	**0.4693**	0.0000	**77.0050**	0.0000	**81.8477**	0.0000
8	25.0494	0.0000	0.0000	0.0000	**0.0030**	0.0000	**0.5707**	0.0000	**81.8477**	0.0000	**86.3323**
9	28.1718	0.0000	0.0000	0.0000	0.0000	**0.0040**	0.0000	**0.6730**	0.0000	**86.3323**	0.0000

Fig. 1(b)) we have to find a universal pulse to induce simultaneously nine transitions between the state pairs, which are shown in Eq. (2), i.e., $|11\rangle \rightarrow |10\rangle$, $|20\rangle \rightarrow |22\rangle$, and so on. In practice, the accuracy of the obtained pulse is assessed by the cumulative transition probability $P = \sum_1^K |\langle\psi^k(T)|\Psi_{\nu'}^k\rangle|^2/K$, which is the first term in Eq. (4). Another quality used to assess the optimized pulse is gate fidelity: $F = |\sum_1^K \langle\psi^k(T)|\Psi_{\nu'}^k\rangle|^2/K^2$. Note that in the F expression different overlaps are added coherently, which takes into account the phase information. One way of enforcing the global phase alignment in the OCT calculations is to add one more superposition transition to the training set.[31] Such a superposition state transition is utilized in Section 5.3 to implement the ternary Shor's algorithm.

5. Results and discussion

The ternary Hadamard gate ($H^{(3)} \otimes I^{(3)}$) and TCNOT (Eq. (2)) are separately implemented and analyzed in Sections 5.1 and 5.2. They are the elemental gates of the improved ternary Shor's order-finding quantum circuit (Eq. (3)), which is then implemented and analyzed in one step in Section 5.3.

5.1. Ternary Hadamard gate

The first stage of order-finding is applying a ternary Hadamard gate to the argument register initially in the state $|0\rangle$ and the function register is uninfluenced, i.e., $H^{(3)}|00\rangle \rightarrow (1/\sqrt{3})(|0\rangle + |1\rangle + |2\rangle)|0\rangle$. The encode scheme is shown in Table 1. The field optimized for $H^{(3)}|00\rangle$ is shown in Fig. 2(a). Several calculations are carried out with different T values. When the optimal duration of the pulse set to 15 μs, $P = 0.9991$ are obtained. The field amplitude does not exceed 6.5 mV/cm. The envelope of the pulse is smooth; however, the pulse shape is complicated. Thus, a standard technique of the FFT (fast fourier transforms) is employed to analyze the frequency content of the pulse. Figure 2(b) shows the spectrum in frequencies. It exhibits a primary spectral structure that covers $|00\rangle \rightarrow |01\rangle$, $|01\rangle \rightarrow |02\rangle$, ..., $|12\rangle \rightarrow |20\rangle$ transitions, which are shown with dotted lines correspondingly.

The frequency spectrum clearly corresponds to control of the ladder state transformations which are shown in Fig. 3. In this case, the population of the initial state $|00\rangle$ should be transferred in equal amounts to the three final states. In the first 5 μs the decrease of population of state $|00\rangle$ mirrors the increase of population of state $|01\rangle$. Then, state $|02\rangle$ starts receiving population from state $|01\rangle$, thus the population of state $|02\rangle$ increases while that of state $|01\rangle$ decreases. Such phenomenon is still demonstrated by the following consecutive state pairs. This is achieved by inducing a ladder of consecutive state-to-state transitions, which is based on the dipole moments summarized in Table 1. At the end of the pulse, each of the final states is expected to receive the population of $1/3$ and the middle states are back to zero. Figure 3(b) shows the time evolution of population in the three upper vibrational states, which are shown in logarithmic scale. At this scale the curves in Fig. 3(b) exhibit some negligible residual population compared with that in Fig. 3(a). Figure 3(c) shows the average probability and the fidelity of the gate for transforming the initial state $|00\rangle$, i.e., $K = 1$. Therefore, they exhibit the same convergence characteristic.

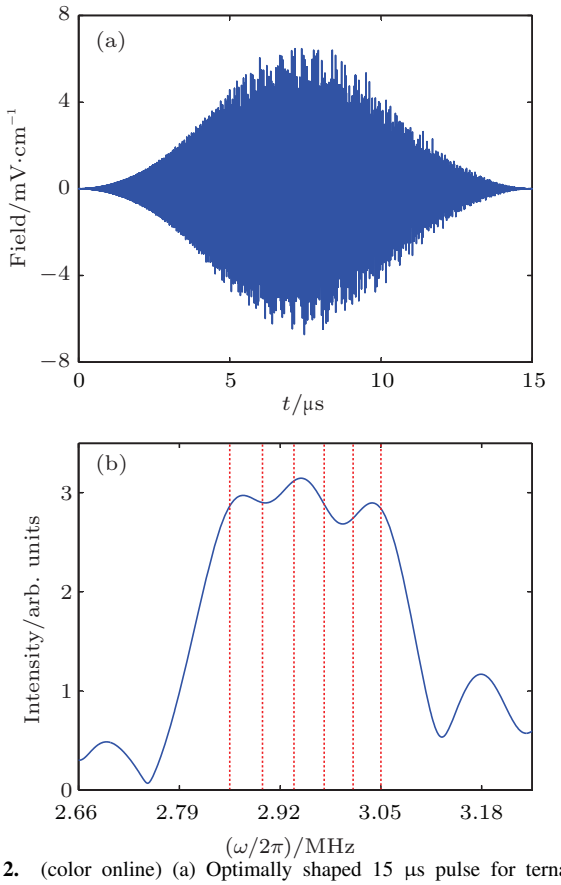


Fig. 2. (color online) (a) Optimally shaped 15 μs pulse for ternary Hadamard gate implemented in the model system. (b) Results of Fourier transform of the optimized pulse.

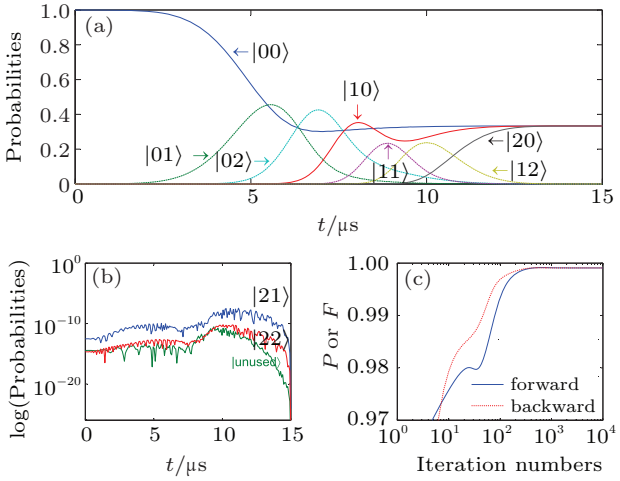


Fig. 3. (color online) Ternary Haramard gate in the model system. (a) Switching of population between the qutrit states during $H^{(3)}|00\rangle \rightarrow (1/\sqrt{3})(|0\rangle + |1\rangle + |2\rangle)|0\rangle$. (b) Populations of the three upper vibrational states during the ternary Haramard gate remain small and their residual populations are negligible. (c) Fidelity and average probability of the gate.

5.2. TCNOT gate

The second stage of order-finding is to apply the TCNOT gate to the registers contain the outputs of the first stage. According to Eq. (3), nine transformations should be involved simultaneously in the field optimization. In addition, it should also be remembered that quantum system can be in any superposition of these states, and the field pulse should also be able to transform appropriately the superposition state. This is absolutely necessary to increase the fidelity of control since a common phase is enforced for all transitions and the resultant field pulse is indeed capable of carrying out a unitary and coherent transformation of any arbitrarily chosen state.[31] Hence, ten transformations, including an extra equally weighted superposition of states

$$\frac{1}{3}\sum_{v,v'=0}^{2}|vv'\rangle \rightarrow \frac{1}{3}\sum_{v,v'=0}^{2}|vv'\rangle,$$

are optimized simultaneously.

Figure 4 shows the state to state transitions which can be divided into four representative categories: (i) The first three columns in Eq. (3) are typical since they are similar to the identity matrix. However, from Figs. 4(a)–4(c) we can see that the transitions from the initial states to themselves are not straight forward. In Fig. 4(a), the population in states $|00\rangle$ and $|01\rangle$ are nearly 0.1 and 0.9 at about 20 μs, respectively. However, they return to the initial values at the end of the pulse duration. Figures 4(b) and 4(c) show the same phenomenon, while the probability variations during $|02\rangle \rightarrow |02\rangle$ in Fig. 4(c) is smaller. (ii) Probabilities exchange between adjacent states, which are shown in Figs. 4(e)–4(h). In Fig. 4(e), probability of state $|11\rangle$ is equal to 1 at the beginning. During the pulse its probability decreases and the probability in state $|10\rangle$ increases. The lower vibrational state $|02\rangle$ also increases slightly and then returns back to zero at the end of the action. (iii) Transitions characterized by $\triangle v = \pm 2$. Figures 4(d) and 4(i) are the attribute of this category. According to Table 1, the dipole moments are clearly dominated by odd step transitions. Such a property suggests that two quanta of vibration in the model system might be easier to achieve by introducing a ladder of consecutive state transitions. For example, figure 4(d) shows that in the first 20 μs of the pulse action, transition is induced and population of the initial state $|10\rangle$ is converted almost entirely into population of the state $|11\rangle$. Then, transition to state $|12\rangle$ starts showing up and the increase of population in state $|12\rangle$ mirrors the decrease of population in state $|11\rangle$. (iv) The evolution of the superposition state, which is shown in Fig. 4(j).

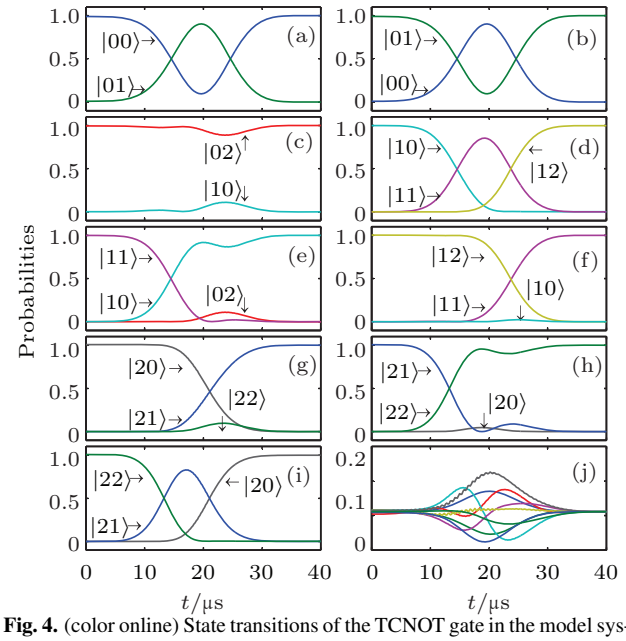


Fig. 4. (color online) State transitions of the TCNOT gate in the model system. (a)–(i) Switching of population between the two-qutrit states during the evolution according to Eq. (3). Note that only the states with population variation are shown. Populations of the other states in each window are small and negligible since they are the same scale with that in Fig. 3(b). (j) Population switching during the evolution of the equally weighted superposition of states.

A convergence study is carried out to make sure that the results are reliable. Figure 5(a) shows the average transition probabilities of forward and backward propagations of the TCNOT gate. The results converge within about 6000 iterations. Both transitions are controlled up to 0.998. Figure 5(b) shows the gate fidelity, 0.965, which is lower compared to the corresponding P caused by the phase error.[31] The optimized pulse is summarized in Fig. 6, which is simple with the maximum amplitude about 2.5 mV/cm. Such an amplitude scale is easy to achieve in experiments. The frequency contents of the pulse are analyzed in this subsection. According to Fig. 4, primary transitions occur between state pairs $|00\rangle$ and $|01\rangle$ (Figs. 4(a) and 4(b)), $|02\rangle$ and $|10\rangle$ (Figs. 4(c) and 4(e)), $|10\rangle$ and $|11\rangle$ (Figs. 4(d) and 4(e)), $|11\rangle$ and $|12\rangle$ (Figs. 4(d) and 4(f)), $|20\rangle$ and $|21\rangle$ (Figs. 4(g) and 4(i)), and $|21\rangle$ and $|22\rangle$ (Figs. 4(g)–4(i)). The six analytical transition frequencies (Table 1) are shown with red dotted lines. In practice, the frequency spectrum of the obtained pulse is slightly different (see Fig. 6(b)). However, six crests in the primary spectrum are distinct. This happens because the ladder of consecutive state transition is not as strict as the presence of the dipole moment between state indexes ± 3, ± 5.

Up to now, the gates, $H^{(3)} \otimes I^{(3)}$ and TCNOT, in Fig. 1(b) have been achieved independently. A straightforward way to implement the ternary quantum algorithm is orderly applying the optimized pulses obtained in Sections 5.1 and 5.2 to the ion trapped in the model system. The Inv$H^{(3)}$ can be achieved in the same way as introduced in Section 5.1. There is a drawback of such serial manipulation: phase alignment between the

gates would be critical and may limit the fidelity of the optimization. This problem can be alleviated by implementing the entire quantum circuit in one single step, which is introduced in detail in the following Section 5.3.

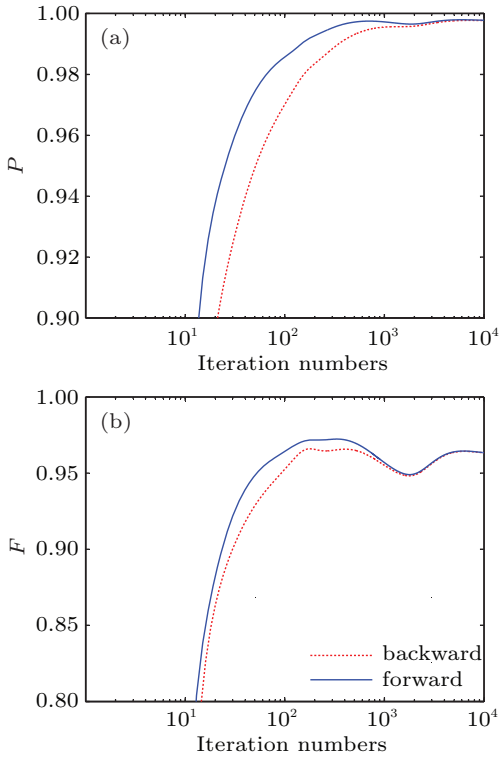


Fig. 5. (color online) (a) Average probability of the TCNOT gate. (b) Fidelity of the gate as a function of iteration numbers.

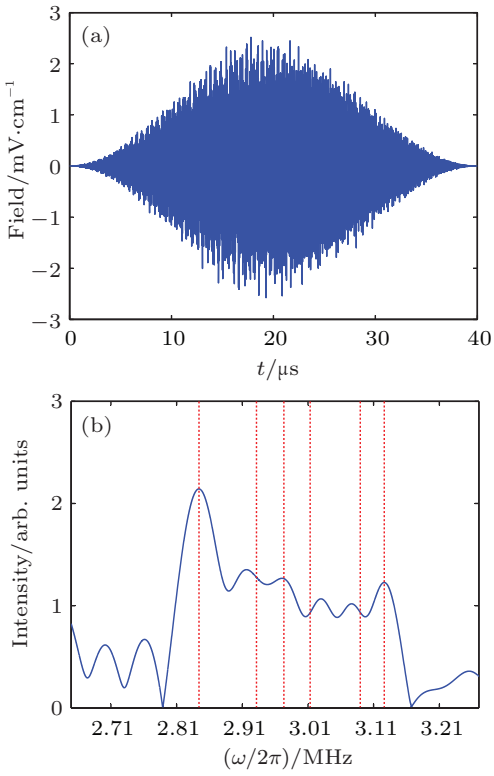


Fig. 6. (color online) (a) Optimally shaped 40 μs pulse for the TCNOT gate implemented in the model system. (b) Results of Fourier transform of the optimized pulse.

5.3. Ternary Shor's order-finding

The entire ternary quantum order-finding algorithm, i.e., equation (4), is implemented in one single step. In order to compare the optimization performance with and without involving the equally weighted superposition of states transition ($\sum_{v,v'=0}^{2}|vv'\rangle/3 \rightarrow \sum_{v,v'=0}^{2}|vv'\rangle/3$), we have implemented two groups of optimization. The average probabilities and fidelities are summarized in Fig. 7. The results converge within about 3000 iterations. For the transformations of the two different training sets, the characteristic probabilities are 0.9943 and 0.9919, respectively, which are shown in Figs. 7(a) and 7(b). However, there is a tremendous difference in the characteristic fidelities. The fidelity in Fig. 7(c) is low (maximum 0.17) due to the serious phase error, while it increases to 0.9630 after introducing the superposition state transition. This conclusion validates the feasibility of the method proposed in Ref. [31] to enforce the global phase alignment in the OCT calculations. Although such fidelity is not very high, in our opinion, this is favorable, taking into account the number and complexity of the state transformations.

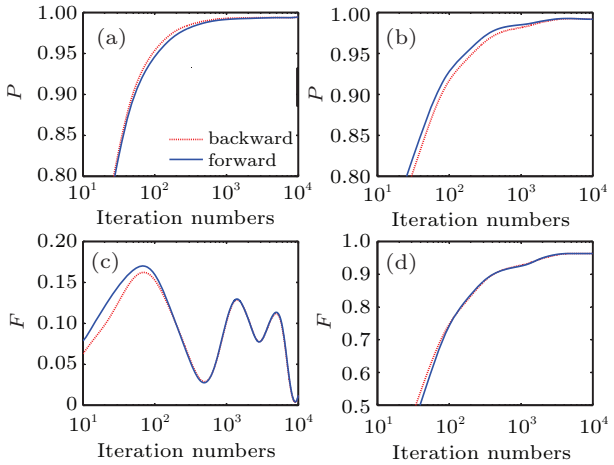


Fig. 7. (color online) (a) Convergence of iterations and average probabilities of the ternary order-finding algorithm without involving the equally weighted superposition of states transition. (b) Convergence with involving the equally weighted superposition of states transition. (c) Fidelity of pulse for simultaneously optimizes nine state transformations. (d) Fidelity of pulse for simultaneously optimizes ten state transformations.

In the following, we analyze the state-to-state transitions. According to Eq. (4), each initial state should be transferred in equal amount to all of the nine states. Thus, all of the final states are expected to receive the population of $1/9$ at the end of evolution. In addition, the evolution of each of the state populations is similar. We analyze the population transformation of initial state $|00\rangle$ for clarity. Another reason for selecting the state $|00\rangle$ is that such a state is actually the input state of Shor's algorithm.[12] The evolution of the equally weighted superposition of states is similar to Fig. 4(j), we do not repeat it again.

The evolution of $|00\rangle$ is shown in Fig. 8. In the first 12 μs, the decrease of population of state $|00\rangle$ mirrors the increase of

population of state $|01\rangle$. During the time interval near $t\sim$12–20 μs, the decrease rate of state $|00\rangle$ becomes larger than the increase rate of state $|01\rangle$. The corresponding population variations are 0.5296 and 0.3692, respectively. This means that state $|01\rangle$ receives less population than that which state $|00\rangle$ releases. This population gap is transferred to state $|02\rangle$ from state $|01\rangle$. It can be seen from this that state $|02\rangle$ starts receiving population at about $t = 12$ μs, which is earlier than the maximum population of state $|01\rangle$ shows up. According to Table 1, the dipole moment between upper states transition is larger than that of lower states, such as the matrix element in Table 1 $M_{1,2} = 42.5473er_0$ is larger than the element $M_{0,1} = 30.3181er_0$. In addition, although the dipole moment for $\triangle\pm3$ transition is small, it still attributes the population transfer. These two reasons mean that the ladder of consecutive state transition is not very strict. For example, state $|10\rangle$ starts receiving population at about $t = 17$, which is also earlier than the maximum population of state $|02\rangle$ shows up. The same scenario repeats again and again for the following vibrational states transferring. State $|11\rangle$ starts receiving population at $t = 20$, $|12\rangle$ start at $t = 23.5$, ..., $|22\rangle$ start at $t = 35$. During the time interval near $t \sim$ 20–40 μs, the population oscillates between the nine encoded states. At the end of the optimization, the final populations of all of the encoded states are all equal 1/9. Note that $|\text{unused}\rangle$ state is expected to be unpopulated, which is shown in Fig. 8 with a scale of 10^{-7}.

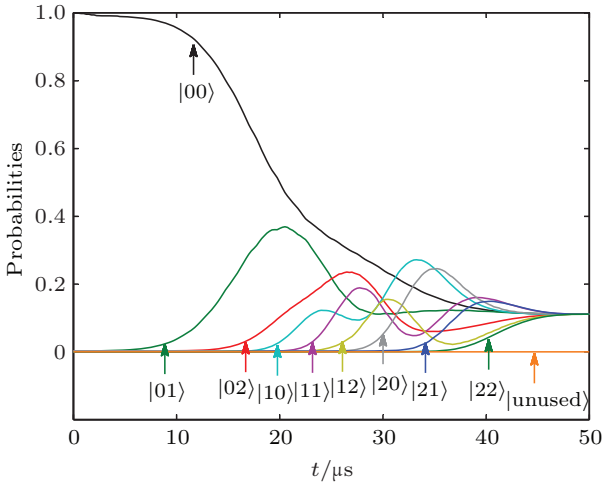


Fig. 8. (color online) Time evolution of state $|00\rangle$ of the ternary Shor's order-finding algorithm.

The optimized field is shown in Fig. 9(a). The duration of the pulse is 50 μs, which is well within the limits of typical coherence time in the modern ion traps (100 ms range[1]). The maximum amplitude is 4.5 mV/cm. Frequency contents are also primary interested. According to Fig. 8, all of the nine encoded states are involved in the ladder of population transition. Figure 9(b) shows a primary spectral structure that covers the eight transition frequencies. Similar to Fig. 6(b), eight analytical transition frequencies (Table 1) are shown with red dotted lines. In practice, the frequency spectrum of the obtained pulse is also slightly different to the analytical values. However, eight crests in the primary spectrum are evident. This happens because the ladder of consecutive state transition is not very strict.

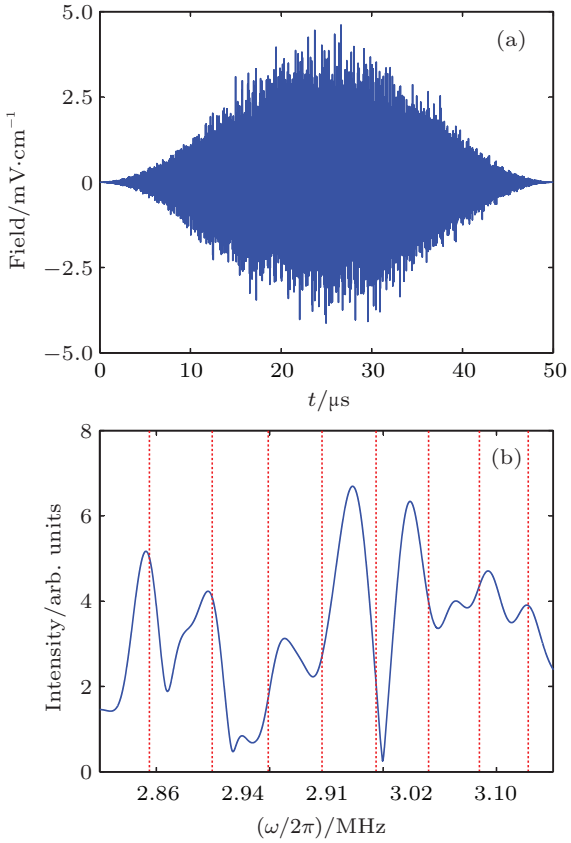


Fig. 9. (color online) (a) Optimally shaped 50 μs pulse for the ternary order-finding algorithm implemented in the model system. (b) Results of Fourier transform of the optimized pulse.

6. Conclusion

In this paper we have explored the scalability of quantum computing in higher-dimensional Hilbert space. Since a bigger space enables us to significantly reduce the required number of elemental gates, a ternary Shor's algorithm for specifically factorizing 21 is implemented using two qutrits. The two-qutrit quantum circuit consists of only three gates, which is encoded into the vibrational states of a single ion trapped in anharmonic potential. Such a trapped ion system is an appropriate model to study higher-dimensional quantum computing. In the model system an optimal control theory is employed to achieve the specific ternary Shor's algorithm in one step. Our numerical simulation results show that accuracy of 0.9919 is achieved. A larger number of iterations would improve the accuracy of the transformation even further. Although the implementation of the ternary algorithm is aiming at a small number, it is still a necessary step on the path towards scalable quantum computing.

Acknowledgments

We thank Prof. Babikov Dmitri and Wang Lei of Marquette University for their feedback.

References

[1] Ladd T D, Jelezko F, Laflamme R, Nakamura Y, Monroe C and O'Brien J L 2010 *Nature* **464** 45
[2] Perez-Delgado C A and Kok P 2011 *Phys. Rev. A* **83** 012303
[3] Xia Y, Song J, Lu P M and Song H S 2011 *J. Phys. B: At. Mol. Opt. Phys.* **44** 025503
[4] Van Meter R and Horsman C 2013 *Communications of the ACM* **56** 84
[5] Monroe C and Kim J 2013 *Science* **339** 1164
[6] Islam R, Senko C, Campbell W C, Korenblit S, Smith J, Lee A, Edwards E E, Wang C C J, Freericks J K and Monroe C 2013 *Science* **340** 583
[7] Zheng S B 2014 *Phys. Rev. A* **89** 022314
[8] Beckman D, Chari A N, Devabhaktuni S and Preskill J 1996 *Phys. Rev. A* **54** 1034
[9] Vandersypen L M K, Steffen M, Breyta G, *et al*. 2001 *Nature* **414** 883
[10] Lanyon B P, Weinhold T J, Langford N K, *et al*. 2007 *Phys. Rev. Lett.* **99** 250505
[11] Politi A, Matthews J C F and O'Brien J L 2009 *Science* **325** 1221
[12] Nielsen M A and Chuang I L 2000 *Quantum Computation and Quantum Information* (Cambridge: Cambridge University Press) pp. 13–17
[13] Klimov A B, Guzman R, Retamal J C and Saavedra C 2003 *Phys. Rev. A* **67** 062313
[14] Zheng S B 2013 *Phys. Rev. A* **87** 042318
[15] Jaime A 2012 *Proc. SPIE Information Optics and Optical Data Storage* II, November 21, 2012, Beijing, China
[16] Li H Y 2013 *Application of Qudits in Quantum Computing and Their Physical Pealizations* (Ph.D. Thesis) (Changsha: National University of Defense Technology) (in Chinese)
[17] Lanyon B P, Barbier M, Almeida M P, Jennewein T, Ralph T C, Resch K J, Pryde G J, O'Brien J L, Gilchrist A and White A G 2009 *Nat. Phys.* **5** 134
[18] Liu K, Li W D, Zhang W Z, Shi P, Ren C N and Gu Y J 2012 *Acta Phys. Sin.* **61** 120301 (in Chinese)
[19] Zhao M and Babikov D 2008 *Phys. Rev. A* **77** 012338
[20] Lin G D, Zhu S L, Islam R, Kim K, Chang M S, Korenblit S, Monroe C and Duan L M 2009 *Eur. Phys. Lett.* **86** 60004
[21] Brown K R, Ospelkaus C, Colombe Y, Wilson A C, Liebfried D and Wineland D J 2011 *Nature* **471** 196
[22] Carsjens M, Kohnen M, Dubielzig T and Ospelkaus C 2013 *Appl. Phys. B* **114** 243
[23] Liu W, Chen S M, Chen P X and Wu W 2013 *Chin. Phys. Lett.* **30** 123702
[24] Ji W B, Wan J Y, Cheng H D and Liu L 2012 *Chin. Phys. B* **21** 063701
[25] Shi Z C, Xia Y, Sone J and Song J 2012 *Quan. Inf. Comput.* **12** 215
[26] Eleanor R and Wolfgang P 2000 arXiv: quant-ph/9809016v2
[27] Wang L and Babikov D 2012 *J. Chem. Phys.* **137** 064301
[28] Zhu W, Botina J and Rabitz H 1998 *J. Chem. Phys.* **108** 1953
[29] Babikov D 2004 *J. Chem. Phys.* **121** 7577
[30] Gollub C, Troppmann U and Vivie-Riedle R 2006 *New J. Phys.* **8** 48
[31] Zhao M and Babikov D 2006 *J. Chem. Phys.* **125** 024105